Synergy of Hydration and Microstructural Properties of Sustainable Cement Mortar Supplemented with Industrial By-Products

E. P. Sumukh [1], B. B. Das[2*], Salim Barbhuiya[3]

[1]Research Scholar, Sustainable Construction and Building Materials Laboratory, Department of Civil Engineering, National Institute of Technology Karnataka, Surathkal, Karnataka, India, 575 025,
Email: sumukhgowdaekkeri@gmail.com, sumukh.197cv500@nitk.edu.in

[2]Professor, Department of Civil Engineering, National Institute of Technology Karnataka, Surathkal, Mangaluru - 575 025, India. Email: bdas@nitk.edu.in

[3]Senior Lecturer, Department of Engineering and Construction, University of East London, E16 2RD, United Kingdom. Email: S.Barbhuiya@uel.ac.uk

[*]Corresponding author email: bibhutibhusan@gmiail.com

Highlights

- Fineness of bottom ash along with the occurrence of silica and alumina played a chief role in performance enhancement of bottom ash-based cement mortars.
- Similarly, the fineness of slag sand along with the availability of additional portlandite generated, assists in undergoing secondary hydration reactions effectively in slag sand-based cement mortars.
- The ability of the finer fraction of IBPs to undergo secondary hydration reactions was confirmed through advanced characterisation studies.

Abstract

The present research assists in resolving the issues allied with the disposal of industrial solid wastes/industrial by-products (IBPs) by developing sustainable IBPs based cement mortars. The applicability of IBPs as a feasible alternative to river sand in cement mortar has been evaluated by investigating the synergy among the ingredients, resulting engineering properties and microstructural developments at early and late curing ages. The study could effectively substitute 30% volume of river sand with bottom ash and 50% in the case of slag sand mortars. The experimental outcomes disclose that the practice of IBPs as fine aggregate enhances the engineering properties of mortar and the optimum replacement level lies at 10% and 40% usage of bottom ash and slag sand, respectively. The advanced characterization studies and particle packing density illustrate the refinement of pores by void filing action and accumulation of additional hydration products through secondary hydration reactions. The consumption of portlandite followed by increased hydration products formation observed through thermogravimetric analysis, X-ray diffraction analysis and energy dispersive X-ray spectroscopy that confirmed the contribution of finer fractions of IBPs to secondary hydration reactions. This constructive development was also observed from the lowering of wavenumber corresponding to Si-O-Si/Al vibration bands in Fourier transform infrared spectroscopy spectra. The improved microstructure resulted in enhancing the compressive strength by 9.01% and 18.18% in optimized bottom ash and slag sand mortars, respectively at the curing age of 120 days. Similarly, the water absorption reduced by 1.03% and 1.24% in bottom ash and slag sand mortars, respectively.

Keywords: Industrial by-products, mortar, hydration, particle packing, microstructure, sustainability.

1. Introduction

Construction industry is one among the leading sectors that greatly contribute to the progress of global economic development [1]. Especially for developing countries, there is a vast scope available for its growth relying on industrialization and urbanization. To achieve these mammoth targets, a huge quantity of construction materials is going to be required. Construction sector being a key for the growth of a country, simultaneously it has also got a negative impression towards the ecological balance of nature by depleting the natural resources, polluting the surface, deforestation, carbon footprint etc. As a result of this, many of the resources may run scarce thereby making the construction sector highly expensive. The main reason associated with the aforementioned issues is that the construction industry routines cement based composites like concrete, mortar etc. for its activities which consume conventional materials like ordinary Portland cement (OPC) as binder, river sand as fine aggregate and crushed granite rocks as coarse aggregate. The chief ingredient of concrete/mortar is aggregates which account for about 70% of the volume [2]. These aggregates used in the production of concrete/mortar are being mined from sources such as river beds (i.e., for sand as fine aggregate) and rock quarries (for coarse aggregates and also for fine crushed aggregates (i.e., M-sand). Mining of aggregates from river beds leads to serious environmental impacts shattering the ecological balance [3–5] and one of the consequences being mining of sand from the river beds is already being prohibited in several provinces. As of now, fine crushed granite rocks (manufactured sand, i.e., M-Sand) have largely replaced the river sand in the construction industry. Even though M-Sand showed satisfying performance as an alternative to river sand [6, 7], it has certain disadvantages in fulfilling the performance requirements of concrete such as grading requirements, workability [8], surface finishing ability [9–11], compressive strength, density, yield, etc. Thus, the natural resource of aggregate is depleting rapidly due to the high consumption worldwide. As a result of these, scarcity of good quality river sand and ill effects of dredging on the environment, researchers are striving to identify and characterize sustainable alternative materials to substitute river sand.

On the other hand, sustainable construction mainly intends to reduce the harmful impacts on the environment caused by the construction industry. Rapid industrialization results in the generation of various kinds of waste which can be hazardous to the environment. Numerous wastes and by-products were being spawned from day-to-day activities such as fly ash, silica fume, agricultural wastes, waste paper sludge ash, pulverized fuel ash, waste molecular sieves, volcanic pumice ash, recycled waste water etc. were used by the researchers as an alternative to conventional materials, as the waste management has become one of the most challenging tasks in the world over a period of time [12–16]. Disposal of these wastes/industrial by-products (IBPs) has created serious problems to the surrounding environment in terms of land occupancy, pollution of the surrounding and subsurface area leading to health hazards. Researches have been conducted by implementing these wastes/IBPs in cementitious systems and reported positively in terms of social need, economic feasibility, engineering properties, durability and microstructure to some extent [17–21]. It is also being reported that the global annual waste accumulation of various other IBPs such as glass waste, E-waste, construction and demolition waste (C & D waste), foundry sand and municipal solid waste, accounted for around 130 million tons, 53.6 million tons, 3 billion tons, 13.38 million tons and 12 billion tons, respectively. These IBPs have occupied thousands of hectares of land throughout the world and many government bodies are promoting their sustainable utilization by possible recycling and reuse. The implementation of these coarser wastes as an alternative to river sand on the performance of cementitious composites is also restricted to some extent of replacement. However, their usage in cementitious composites has shown satisfactory outcomes in terms of hardened properties, but not with respect to the properties at fresh state [22–24].

Presently, coal-fired thermal power stations are accountable for producing huge amounts of coal waste in most developing nations. Bottom Ash (BA) is one of the major industrial by-products which is produced at the bottom of the furnace during the process of coal combustion for generating electricity. These thermal power plants produce large amounts of bottom ash as a by-product. It is usually treated as a solid waste material and is disposed on surface impoundments or in landfills leading to environmental pollution. Slag sand is another major non-metallic industrial by-product from metal smelting processes which is manufactured under controlled conditions. The granulated slag is obtained by the process of quenching the molten slag of the furnace in water. Therefore, a large quantity of bottom ash and slag wastes is getting accumulated near the industrial locality causing serious environmental hazards with time. It is being reported that the global annual waste accumulation of bottom ash and slag sand is about 574 million tons and 300–360 million tons, respectively [25, 26]. However, the effective way of regenerating the values from the IBPs in construction industry is not being suitably developed. Thus, there is a potential need to utilize these IBPs in an effective manner. Concrete and mortar are one among the best possible areas where these IBPs can be largely employed as an alternative material to conventional ingredients.

With the view of developing a sustainable solution, the present investigation explores the possibility of utilizing the industrial by-products such as bottom ash and slag sand as construction material by partially substituting the river sand to check their suitability in cement mortar. To check the performance of resulting cement mortar, studies related to engineering properties and microstructural developments were conducted through advanced characterization techniques.

2. Experimental methodology

2.1 Material used and their properties

Ordinary Portland cement of 53 grade confirming to ASTM C150/C150M-22[27] was used as a binder to produce cement mortar. The fine aggregates used involve 3 kinds of materials namely river sand, bottom ash (BA) and slag sand (SS). River sand confirming to zone II as per IS: 383-2016 was employed and as a partial replacement to river sand, IBPs namely bottom ash and slag sand were used at different replacement levels. For mixing and curing mortars, ordinary potable water confirming to IS 10500:2012 [28] was used. To obtain the desired flow properties in fresh cement mortar, a polycarboxylate ether-based superplasticizer confirming to IS 2645:2003 [29] and IS 9103:1999 [30] was used. The preliminary investigations on these raw materials were carried out to investigate the basic properties as per the guidelines mentioned in the standards. Table 1 shows the extracted properties from the preliminary studies on raw materials and Fig. 1 represents their particle size distribution. The morphology of bottom ash and slag sand was observed through scanning electron micrographs which are presented in Fig. 2 and Fig. 3, respectively. The chemical composition of bottom ash and slag sand is presented in Table 2.

Table 1: Properties of various materials used

Materials		**Properties**				
		OPC	**RS***	**BA**	**SS**	**SP***
Specific gravity		3.11	2.66	2.09	2.61	1.08 ± 0.02
Initial setting time (minutes)		110	-			-
Final setting time (minutes)		170	-			-
Standard consistency (%)		32	-			-
Fineness (m^2/kg)		300	-			-
Soundness (mm)		2	-			-
Loss on Ignition (LOI)		2.30	-			-
Bulk density (kg/m^3)	Loose	-	1500	997	1387	-
	Compacted	-	1598	1075	1465	-

% of Voids	Loose		43.07	52.19	46.87	-
	Compacted	-	39.34	48.44	43.87	-
Fineness Modulus		-	2.47	2.16	2.67	-
Water absorption (%)			0.98	0.83	0.71	
pH		-	-			≥ 6
Chloride content		-	-			< 0.20 %

*- RS: River sand, *SP- Superplasticizer

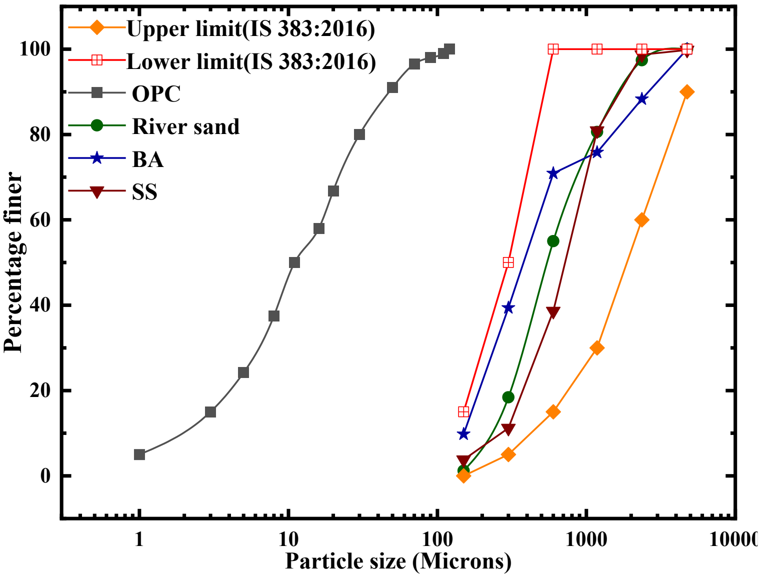

Fig. 1. Particle size distribution of various materials used

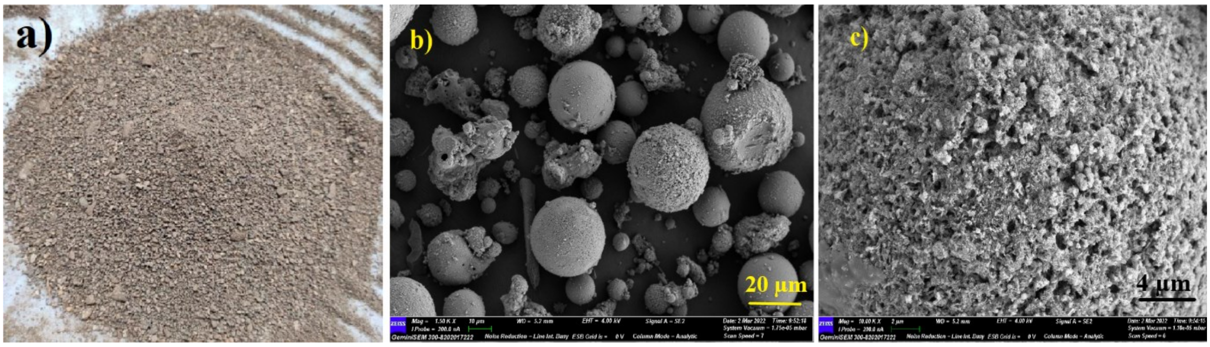

Fig. 2 a) Bottom ash, b) scanning electron micrograph of BA at 1500X, c) scanning electron micrograph of BA at 10000X

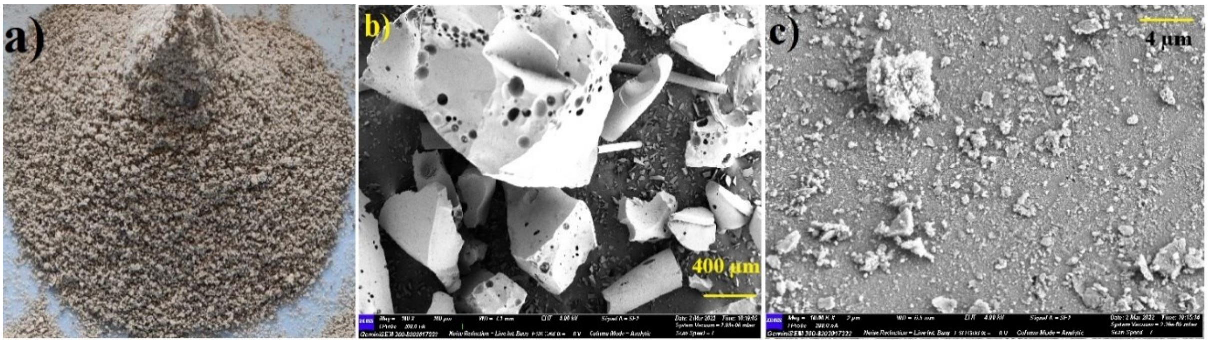

Fig. 3. a) Slag sand, b) scanning electron micrograph of slag sand at 100X, c) scanning electron micrograph of slag sand at 10,000X

The scanning electron micrographs of bottom ash presented in Fig. 2 b) and 2 c) shows that the bottom ash particles are fairly rounded with rough texture. However, the slag sand particles shown in Fig. 3 b) and c) are found to be angular with smooth texture. The particles of slag sand were found to be brighter and whiter which could be due to the presence of excess amounts of calcium-based compounds in them.

Table 2. Chemical compositions of bottom ash and slag sand

Component	% mass	
	Bottom ash	Slag sand
MgO	1.2999	3.9780
Al_2O_3	18.3026	14.6523
SiO_2	46.9721	28.5487
P_2O_5	0.8160	-
SO_3	0.9131	1.4384
K_2O	1.7413	0.6182
CaO	9.6538	45.7530
MnO	0.1280	1.1584
Fe_2O_3	17.5230	1.8056
Na_2O	1.0318	0.1599
Cl	0.0750	0.0166
TiO_2	1.1941	1.3285
Rh_2O_3	-	0.3912
SrO	0.3080	0.1045
ZrO_2	0.0412	0.0468

2.2 Details of cement mortar mixes developed

In the present study, three kinds of mortars were developed to check the feasibility of IBPs as fine aggregate in cement mortar. The mortars, entirely produced with river sand as fine aggregates are considered as control mortar (reference mix) designated by CM. The mortar mixes in which the river sand was replaced by bottom ash are designated by alphabet “B” and similarly “S” for the mortar mixes in which the river sand was replaced by slag sand. The numbers following these alphabets depict the extent of fine aggregate replacement in terms of percentage volume of river sand. A binder-to-fine aggregate ratio of 1:3 and water-to-binder ratio (w/b) of 0.45 was maintained throughout the study. The required corrections related to water absorption and moisture content were taken into consideration while preparing the mortar mixes. A minimum flow value of 150 mm was maintained to ensure better workability using a superplasticizer. Table 3 shows the details of the mixes produced.

Table 3. Details of the mortar mixes produced

Mix designation	Weight (kg/m^3)					SP (% bwob*)
	OPC	RS	BA	SS	Water	
CM	777.50	1943.25	-	-	349.88	0.00
Bottom ash based mortar						
B10	777.50	1795.50	156.38	-	349.88	0.17
B20	777.50	1596.00	312.75	-	349.88	0.40
B30	777.50	1396.50	469.13	-	349.88	1.00
Slag sand based mortar						
S10	777.50	1795.50	-	195.75	349.88	0.05
S20	777.50	1596.00	-	391.50	349.88	0.05
S30	777.50	1396.50	-	587.25	349.88	0.20
S40	777.50	1197.00	-	783.00	349.88	0.20
S50	777.50	997.50	-	978.75	349.88	0.40

*bwob- by weight of binder

2.3 Production of cement mortar samples

The ingredients of the mortar mix were dry mixed manually and further wet mixing was done using an automatic mortar mixer, designed as per the guidelines mentioned in EN 196-1 [31]. The produced mortars were then cast in a mould of size 70.6 mm × 70.6 mm × 70.6 mm. The cast specimens were further allowed to set under a humid environment (i.e., 27 ± 2°C and 95% RH). The cast samples were then given time to set in a humid atmosphere (i.e., 27 ± 2°C and 95% RH) for 24 hours. Later the specimens were demoulded and kept for curing by immersing in normal potable water maintained at 27 ± 2°C till the day of testing. After a curing age of 3, 7, 28, 56 and 120 days, samples were taken out, dried and tested to check their performance in a hardened state. Fig. 4 presents a brief overview of the carried-out study.

2.4 Details of tests performed

2.4.1 Fresh and hardened properties

The workability and setting time of the produced mortars were assessed in the fresh state. Whereas the hardened state properties were extracted by making use of destructive and non-destructive methods. All the properties reported in the present study are calculated by considering the average of results collected from three specimens. Table 4 shows the details of the tests performed to assess the fresh and hardened properties.

2.4.2 Microstructural analysis and characterization techniques used

The microstructure of cement mortar greatly influences their engineering properties and is very crucial to comprehend which helps in understanding the chemistry that is contributing to the performance. Thus, the hydrated mortar samples were collected from the core of mortar specimens after 28 and 120 days of curing. Further, these chunks were kept submerged in isopropanol for about 24 hours to prevent further hydration reactions with time [32, 33]. Soon after that, those chunks were oven dried at a temperature range of 40-60 °C till the weight became stabilized. These prepared samples were then preserved in desiccators along with silica gel pellets, and a vacuum environment was maintained to prevent further absorption of moisture by the samples. These preserved samples were further used to conduct various characterization studies.

The microstructural development in produced mortars was observed by carrying out morphological study using scanning electron microscopy (SEM) technique in secondary electron mode. Further, the elemental composition in these samples was examined through energy-dispersive X-ray spectroscopy (EDS). The mortar samples were gold sputtered and taken further for microstructure assessment through SEM-EDS.

Table 4. Details of the tests performed

Type	Test	Reference	Remarks
Fresh properties	Mini flow table	EN 1015-3 [34]	-Workability/flowability measurement -To fix the superplasticizer dosage required for maintaining a minimum flow diameter of 150 mm
	Setting time	ASTM C403/C403 M-08 [35]	-Initial and final setting time measurement using penetration resistance measurements
Hardened properties	Compressive Strength	IS 4031-Part 6:1988 [36]	-Using a compressive testing machine at a loading rate of 35 MPa/min
	Density	BS EN 1015-10:1999 [37]	-Weight by volume method using weighing balance
	Permeable porosity	[38, 39]	-Vacuum water absorption technique using vacuum desiccators
	UPV	IS 516 (Part 5/sec 1):2018 [40]	-Using portable ultrasonic non-destructive digital indicating tester (PUNDIT)
	Water absorption	BS 1881-122 [41]	-By considering the change in weight at saturated surface dried and oven dried condition

The XRD study was carried out to determine the mineralogical compositions formed in the hydrated cement mortar samples. The preserved samples were ground and sieved through an IS sieve having a mesh size of 75 microns, and the passed fine powdered particles were then used for the study. The XRD tests were carried out in Malvern Panalytical and Jeol-JPX 8P make X-ray diffractometers operated with Cu Ka radiation (40 kV/40 mA) at a scanning rate of 2°/min. The samples were examined at 2θ degrees ranging between 4° to 80° and the recorded XRD results were analyzed using X'Pert High Score Plus software.

The decomposition of various phases associated to hydration products with the temperature was investigated through thermogravimetric analysis (TGA), with the aid of RIGAKU TG-DTA 8112 thermogravimetric analyzer. Further, the hydration products formed in different types of mortars were quantified using the obtained TGA data. The sample preparation method followed for TGA was similar to that followed for XRD study and testing was carried out in a nitrogen purge atmosphere where the temperature varied from room temperature to 875°C. During the course of test, the temperature was increased at a rate of 10°C/min and nitrogen purge rate was kept at 20 ml/min. The quantification of hydration products was done based on their decomposition at particular temperature boundaries in terms of weight loss. The endothermic peaks formed in derivative thermogravimetric curve (DTG) as a result of compound decomposition (in the form of weight loss) determine the temperature boundaries. In the present study, the endothermic peak observed in the temperature range of 400-500°C is considered as the mass loss from the decomposition of calcium hydroxide (CH) [32, 42–45]. Similarly, the temperature boundary associated with the decomposition of calcium carbonate was taken in the temperature boundary of 600-800°C [32, 46]. Further, the amount of water associated with other hydration products (WH) was quantified by considering the weight loss associated with the temperature range of 35-600°C, excluding the decomposition of CH[32, 46].

Fourier transform infrared spectroscopy (FTIR)studies were carried out with Bruker Alpha II make equipment and the data were extracted from the OPUS software. The sample preparation method used is similar to that followed for XRD and TGA analysis. The FTIR spectra were collected in transmittance mode between the wavelengths ranging from 600 cm^{-1} to 4000 cm^{-1} using ATR method. The different hydration phases that are formed during the course of hydration such as portlandite ($Ca(OH)_2$), C-S-H, C-A-S-H, sulfates and carbonate phases (such as ettringite, monosulfoaluminate, sulfoaluminate, calcium carbonate) etc., were studied based on recorded peaks with intensities and their wavenumber shifts over the age of curing.

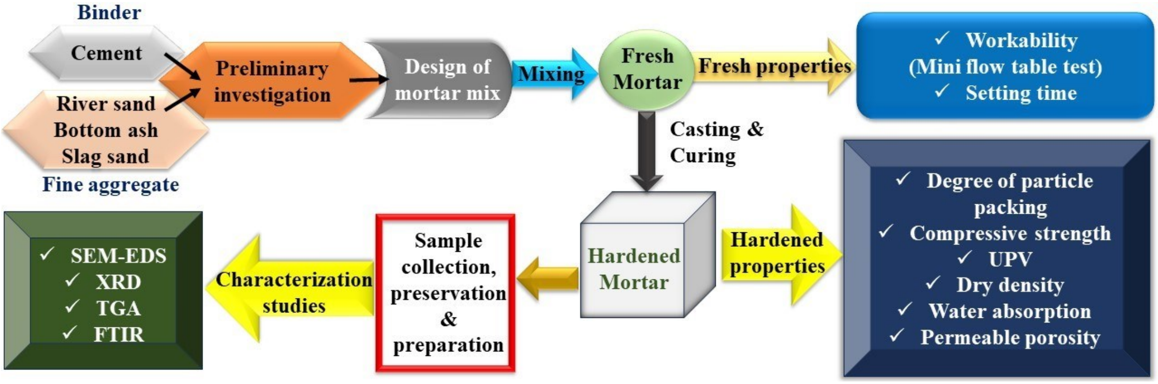

Fig. 4. Flowchart showing the details of the study

3. Analysis of results and discussions

3.1 Particle packing in the developed cement mortars

Modified Andreasen and Andersen packing model was employed in the present study using "EMMA" software to check the degree of particle packing achieved in the produced mortars[47]. A distribution coefficient (q) of 0.30 suitable for attaining medium workability was chosen for the analysis[32]. The particle packing curves of BA based and SS based mortars are presented in Fig. 5. The obtained particle packing curves depict that the particle packing density is enhanced with the implementation of IBPs as a partial alternative to river sand. The improvement in the extent of fitting (R^2) of IBPs based mortars particle packing curves, calculated with respect to the target curve (fixed by the modified Andreasen and Andersen packing model) confirms the increment of particle packing density[48].

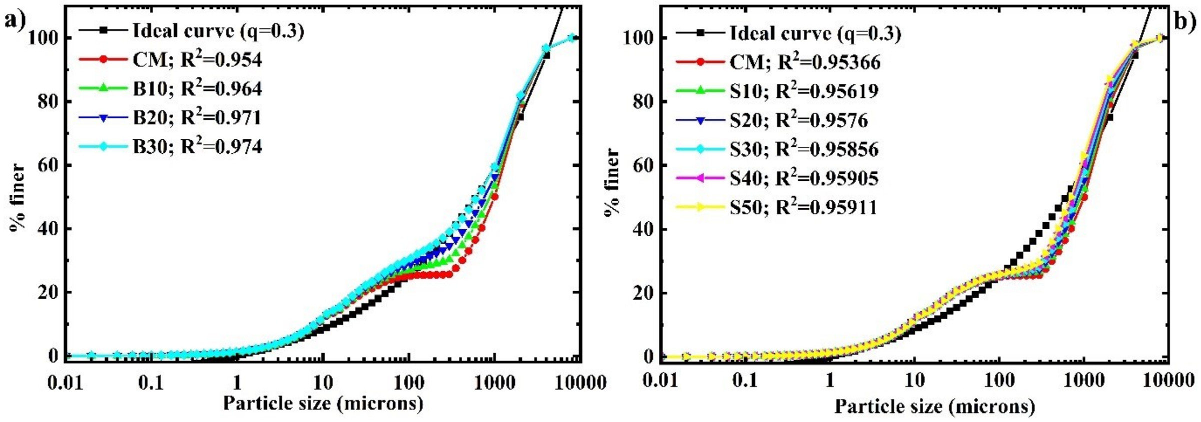

Fig. 5. Particle packing curves for a) Bottom ash based mortars and b) Slag sand based mortars

3.2 Fresh properties

3.2.1 Workability

Workability of produced cement mortar mixes with varying dosages of BA and SS is presented in Fig. 6 a) (BA based mortar) and Fig. 6 b) (SS based mortar) which consists of flow diameter, flow value and their corresponding dosage of superplasticizer consumption.

By observing the results obtained, it can be noted that the addition of BA into the mortar mix as a substitute to river sand reduces the flow characteristics. This behavior can be observed through the increased dosage of superplasticizer consumption with the percentage usage of BA. The control mortar (CM) produced entirely with river sand as fine aggregate achieved the required minimum flow diameter of 150 mm without consuming any superplasticizer. With the percentage usage of BA, the flow characteristics were observed to become poorer due to the intrinsic properties of BA. The rough textured BA particles (which can be observed through SEM images in Fig. 2 c)) increase the friction between the particles, thereby resisting the movement of particles over one another. Also, the fine nature of BA particles as compared to river sand (which can be observed from Fig.1) demands more water for particle surface wetting. Thus, dry and harsh mortar mixes were formed at high volume usage of bottom ash which requires more superplasticizer to achieve the required flow.

Similarly, by observing the superplasticizer dosage requirement and their corresponding flow values in SS based mortars, it can be concluded that the workability of produced mortars tends to reduce with the increasing volume of slag sand. The possible reasons for this reduced workability are, a) the irregularly shaped particles of slag sand (seen in Fig. 3b) restrict the movement of particles over one another, and b) the calcium rich particles of slag sand increase the degree and heat of hydration which makes the mortar mix harsh due to the increased water demand.

It is also important to notice the sudden declination of flowability characteristics and increased superplasticizer consumption in bottom ash and slag sand mortars at a replacement level of 30% and above. This could be due to the formation of harsh mortar under the influence of excessive amounts of fines, due to the increased proportion of IBPs. The fine particles of IBPs tend to fill the void spaces and form cohesive mortar at lower proportions till 20% replacement volume. The occurrence of fines in relatively higher volume at higher replacement levels (30% and above) enhances the water demand and reactivity which affects the overall flow characteristics.

3.2.2 Setting time

The influence of using IBPs such as BA and SS on the setting time of cement mortar is presented in this section. Fig. 6c) and Fig. 6d) depict the graphical representation of setting times recorded for different BA and SS based cement mortars respectively.

By observing the results shown in Fig. 6c), it can be seen that the bottom ash addition in the cement mortar as a partial substitute to river sand retards the hydration process which can be seen from the increased setting time values. This could be due to increased concentration of silica and alumina in the cement mortar by the usage of bottom ash, which reduces the heat of hydration and further prolongs the hydration mechanism. Whereas, in case of SS based cement mortar mixes, both initial and final setting time was found reducing with the increasing replacement level of river sand. This can be attributed to the increased amount of calcium oxide in the cement mortar formed by the addition of slag sand, which intensifies the degree and heat of hydration, resulting in the fast setting of mortar mixes. Also, there could be a possibility of variation in the amount of heat accumulation generated from the hydration reaction in cement mortar mix depending on the heat absorbing capacity of replacement material compared to that of river sand. Thus, the heat absorbing property of bottom ash and slag sand has also influenced the initial and final setting time.

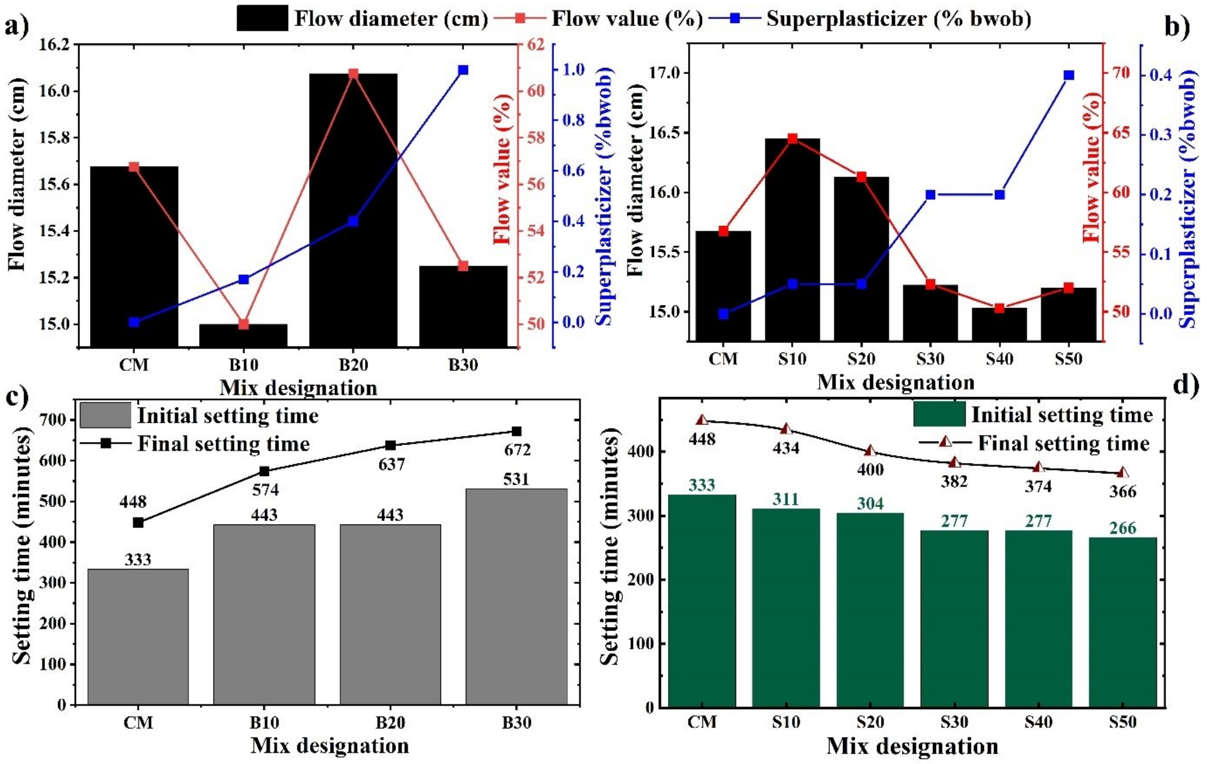

Fig. 6. Flow characteristics of a) bottom ash based cement mortar and b) slag sand based cement mortar; setting time of c) bottom ash based cement mortar and d) slag sand based cement mortar

3.3 Hardened properties

3.3.1 Compressive strength

Compressive strength development in control (CM), BA and SS based mortars were measured at the curing age of 3, 7, 28, 56 and 120 days. Fig. 7a) and Fig. 7d) shows the compressive strength of BA based and SS based cement mortars, respectively.

The compressive strength results obtained from the BA based mortars exhibited a decreasing trend with the increasing replacement level of river sand in the initial days of curing (i.e., till 28 days). This could be attributed to the increased concentration of silica and alumina with the usage of bottom ash in cement mortar which reduces the heat of hydration and further prolongs the hydration mechanism. However, there observed a comparable performance by B10 mortar against CM at almost all the curing ages, owing to the enhanced particle density fashioned by void filling action and possible secondary hydration activity (after 28 days of curing) undergone by finer bottom ash particles. Similarly, the positive influence on using slag sand as a partial replacement material to river sand can be seen through the compressive strength results after 28 days of curing. The improvised particle packing density with the increasing slag sand content (which can be seen in Fig. 5) helped the ingredients of mortar to undergo primary and possible secondary hydration reactions more effectively. Since the slag sand is rich in calcium oxide, siliceous and aluminous compounds, the finer particles of slag sand undergone supplementary hydration reactions (secondary hydration reaction/ pozzolanic reaction) after 7 days of curing, resulting in the formation of additional hydration products. These actions helped in refining the pore structure of mortar mixes in an effective manner leading to the formation of dense microstructure which enhances the hardened mechanical properties such as compressive strength.

It is also important to notice from the results that the bottom ash based and slag sand-based mortars showed optimum performance at about 10% and 40% volume replacement of river sand, respectively. The reduction in the compressive strength beyond the optimized dosage of BA is due to poorer gradational characteristics that caused bleeding and further affected the matrix of the produced mortar. Also, the enhancement in the silica-alumina content by using the BA at higher levels restrains the degree of hydration reactions. Whereas in the case of slag sand-based mortars, the excessive amount of calcium hydroxide generated from the calcium rich slag sand particles caused leaching and also accelerated the early hydration reactions with greater heat of hydration which altogether makes the cement system weak due to the formation of microcracks. At the curing age of 28, 56 and 120 days, S40 mortar recorded 45.36%, 14.40% and 29.83% higher compressive strength than the control mortar respectively. Similarly, B10 mortar showed 2.94% and 9.01% at the end of 56 and 120 days of curing respectively.

3.3.2 Dry density

The dry density of control (CM), BA and SS based mortars were measured at a curing age of 3, 7, 28, 56 and 120 days. Fig. 7 b) and Fig. 7 e). represents the dry density of BA based and SS based mortars, respectively.

The obtained results showed an increasing trend of dry density with the progress in curing age due to continued formation of hydration products which refine the mortar pore structure. It is also important to notice that the dry density of produced mortars reduces with the increasing proportion of BA and SS. This is attributed to lower specific gravity of replacement material (i.e., BA and SS) than that of river sand. The lower specific gravity of a material causes a reduction in the unit weight of the resulting mortar. Even though the fine particles of IBPs increase the particle packing density by filling the void spaces, there observed a reduction in the dry density with the increasing percentage of IBPs, as the variation in the dry density is highly reliant on the specific gravity of the IBPs.

3.3.3 Ultrasonic pulse velocity (UPV)

The uniformity and quality of mortars produced using IBPs were investigated by conducting UPV tests after the curing age of 3, 7, 28, 56 and 120 days. Fig. 7 c) and Fig. 7 f) represents the UPV results of BA based and SS based mortars, respectively.

From the measured values of UPV, there observed an improvement to UPV with the progress in curing age for all types of produced mortars, due to densification of microstructure by hydraulic and pozzolanic reactions. The UPV of control mortar was observed to be higher than any other IBPs based mortars at early ages of curing (i.e., till 7 days). The UPV tends to reduce with the increasing proportion of river sand replacement by IBPs. This could be attributed to the lack of uniformity formed in the mortar by the usage of IBPs, consisting a wide number of minerals. However, the UPV tends to increase with the increasing proportion of slag sand beyond 7 days of curing which could be due to the influence of secondary hydration reactions imparted by slag sand particles that refined the mortars pore structure. It is also important to notice that there observed a gradual fall in the UPV values beyond 40% usage of slag sand at all the curing ages. The generation of cracks due to higher heat of hydration and reduction in the uniformity of the mix at higher proportions of slag sand were the causes for reduced UPV. All the mortars produced recorded a UPV value ranging between 3700 m/s and 4700 m/s by the end of 120 days of curing. Hence the produced mortars were in the category of good to excellent grade quality as per IS 13311:1992 – Part 1 [49].

3.3.4 Water absorption and Permeable porosity

The water absorption and permeable porosity of control and IBPs based mortars were assessed at the end of 3, 7, 28, 56 and 120 days of curing. Fig. 8 a) and Fig. 8 b) presents the water absorption and permeable porosity of BA based mortars, respectively. Similarly, Fig. 8 c) and Fig. 8 d) represents the water absorption and permeable porosity of SS based mortars, respectively.

From the obtained results it can be observed that the water absorption and permeability porosity followed a quite similar trend with the usage of IBPs at all the curing ages. This could be due to the fact that the absorbed water predominantly accumulates in the permeable void spaces or pores present in the mortar mixes and these pore volumes are regarded as porosity. The water absorption and permeable porosity were found reducing with the progress in curing age which is due to the refinement caused to the pore structure of mortar by the generation and accumulation of hydration products.

The utilization of IBPs in mortars as a partial replacement to river sand showed a positive influence on water absorption and permeable porosity. The general trend of water absorption and permeable porosity was found reducing with the increasing proportion of IBPs till the optimum replacement level (i.e., 10% of BA and 40% of SS) and thereafter found increasing. This behavior can be ascribed to the synergetic influence from the improved particle packing and effective secondary hydration reactions with the increasing proportion of IBPs. In addition to these, the lower water absorbing property of BA and SS in comparison with river sand also contributes in reducing the water absorption and permeable porosity of mortar. However, exceeding the dosage of IBPs beyond the optimum percentage caused an increment in the values of water absorption and permeable porosity. This development is due to the increased finer particles in the mortar mix at higher volume of IBPs, which lowers the water availability in mortar for undergoing hydration reactions effectively. The increased composition of silica, and alumina by the usage of BA and increased calcium composition by the usage of SS beyond the optimum requirement also affects the hydration mechanisms leading to the development of weak microstructures in mortar, which increases the water absorption and permeable porosity.

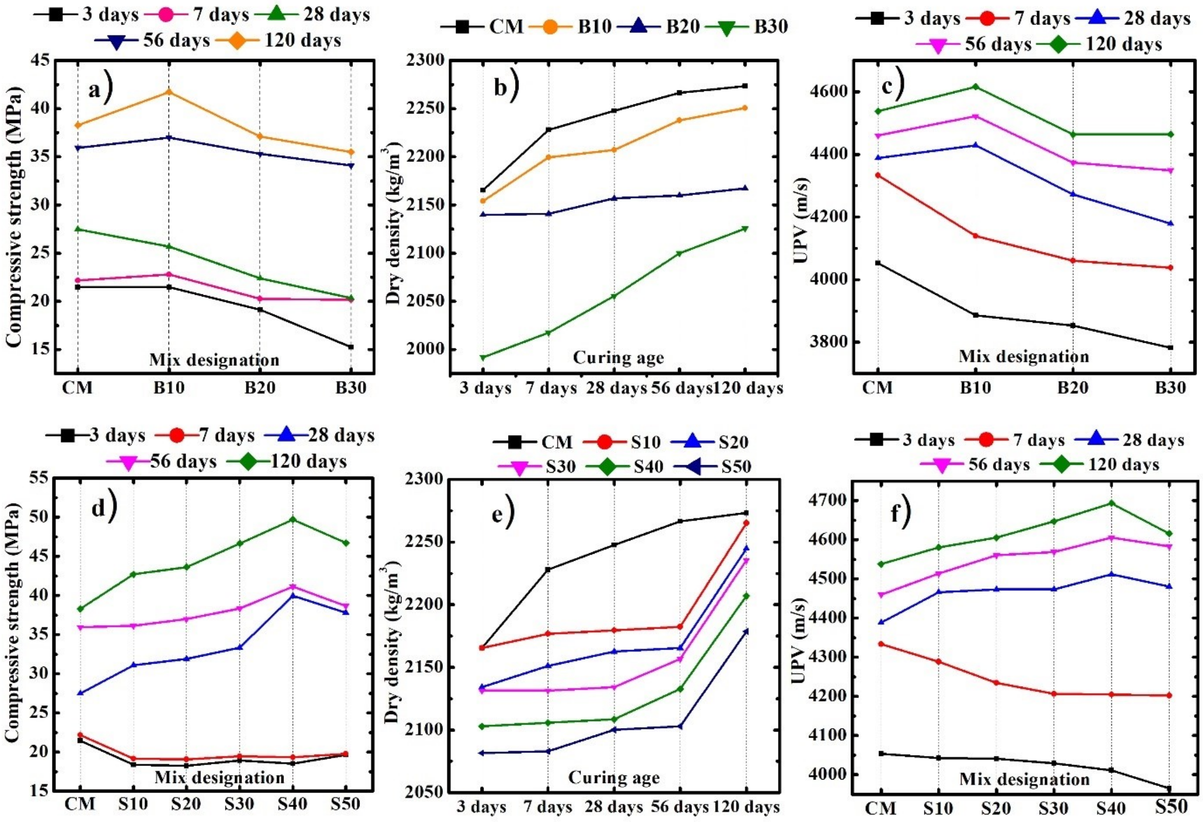

Fig. 7 a) Compressive strength, b) Dry density, c) UPV of bottom ash based cement mortar; and d) Compressive strength, e) Dry density, f) UPV of slag sand based cement mortar

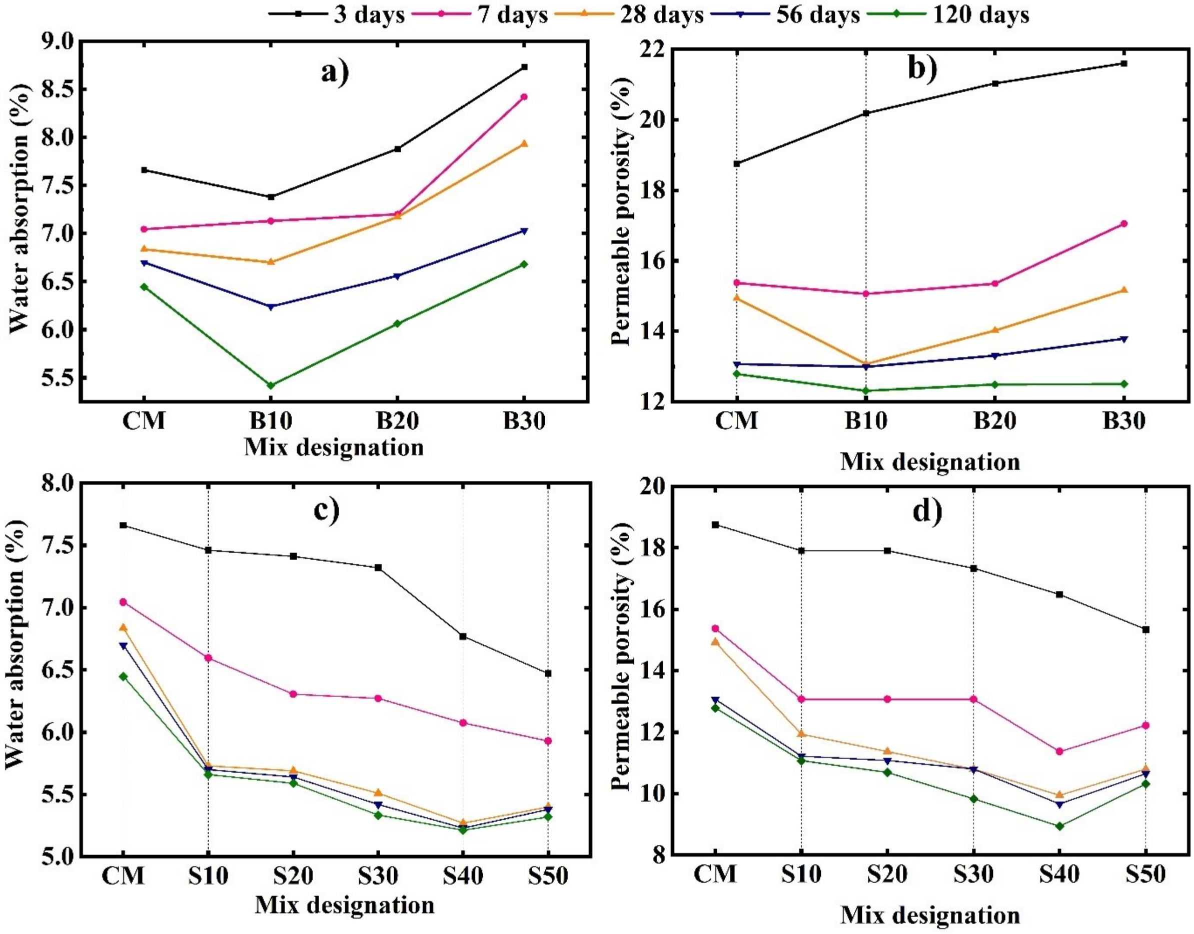

Fig. 8 a) Water absorption, b) Permeable porosity of bottom ash based cement mortar; and c) Water absorption, d) Permeable porosity of slag sand based cement mortar

3.4 Microstructure and characterization studies

3.4.1 Mineralogical characterization

The mineralogical characteristics of hydrated samples of control, BA and SS based cement mortars at a curing age of 28 days and 120 days were investigated with the aid of XRD technique. The XRD analysis was carried out for control mortar and IBPs based mortars till one replacement level beyond the optimum replacement percentage for river sand (i.e., till B20 and S50). The chemical name, empirical formula and peak assignment designations corresponding to various mineralogical compounds detected were tabulated in Table 5.

The XRD patterns of BA based mortar at 28 days and 120 days of curing are depicted in Fig. 9 a) and Fig. 9 b), respectively. Similarly, the XRD patterns of SS based mortar at 28 days and 120 days of curing are presented in Fig. 10 a) and Fig. 10 b), respectively. By observing the XRD patterns of 28 days cured mortar samples, it can be noticeable that the occurrence of portlandite (CH) peaks are more and prominent in BA based mortars. This is due to the delay in hydration process caused by the increased concentration of silica and alumina with the usage of bottom ash. The addition of calcium from the IBPs to the mortar composition also enhances the portlandite formation. However, there observed a preferential formation of additional calcium silicate hydrates and calcium silicate aluminium hydrates through the effective conversion of portlandite into stable hydration products such as CSH and CASH phases in IBPs based mortars. The mineralogical compounds related to CSH and CASH phases such as Gismondine, Chabazite, Tobermorite and Kamaishilite have additionally formed in BA based mortars. Similarly, Gismondine, Kamaishilite, and Hillebrandite were observed in the case of SS based mortar. While in the control mortar (CM), in addition to Xonotlite (CSH), the portlandite (calcium hydroxide; CH) generated were rapidly converted into various other hydration products such as carbonates and sulfate hydrates (Gypsum, Yeelimite etc.) that implement a comparatively weaker microstructure in mortar.

Similarly, by investigating the XRD patterns of 120 days cured mortar samples, it is clear that the peaks corresponding to portlandite are found to be more and prominent which indicates the formation of portlandite content (CH) with curing age. The produced CH in control mortar remains mostly unutilized after 28 days of curing. However, the portlandite produced in the IBPs based mortars was consumed for secondary hydration reactions, leading to the formation of additional hydration products that were detected in the form of mineralogical compounds associated to CSH and CASH. The mineralogical compounds associated to CSH and CASH phases such as Gismondine, Chabazite, Wairakite and Tobermorite were additionally formed in BA based mortars. Similarly, Gismondine, Wairakite, Rosenhahnite, Hillebrandite and Katoite are the compounds that were additionally formed in SS based mortars. It is also important to notice that the XRD pattern of 120 days cured samples appeared less crystalline than that of 28 days cured ones, owing to the effective conversion of mineralogical compounds from crystalline phase to amorphous CSH and CASH phase.

Overall, by analyzing the XRD patterns, it can be concluded that a significantly higher number of mineralogical compounds associated to calcium silicates and calcium aluminium silicates were formed by the application of IBPs in cement mortar with lesser formation of carbonates and sulfates. This development in IBPs mortars facilitated to perform better than control mortar which can be seen through the measured engineering properties such as compressive strength, water absorption and permeable porosity.

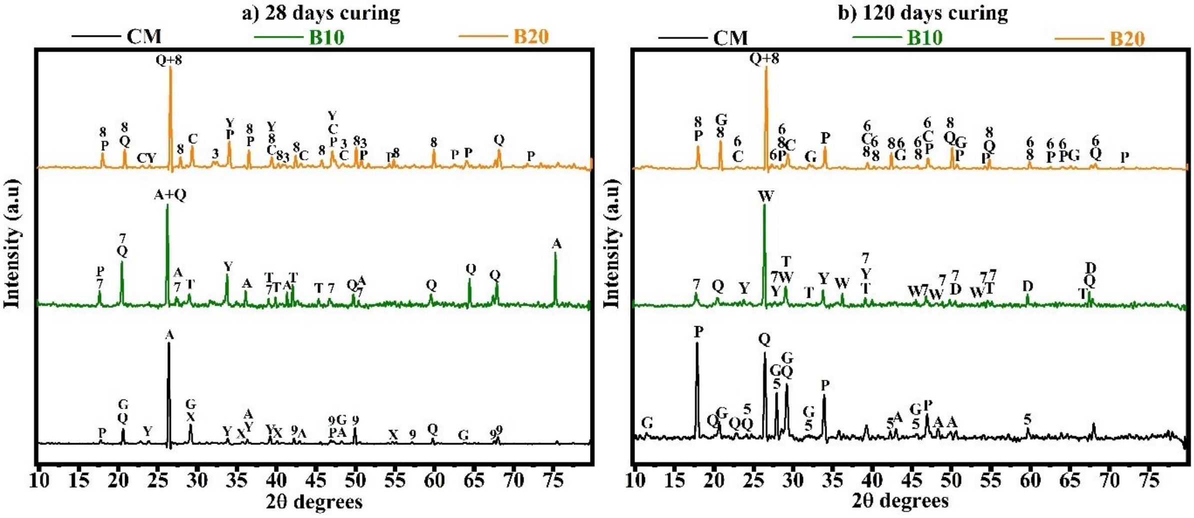

Fig. 9. XRD pattern of bottom ash based cement mortar

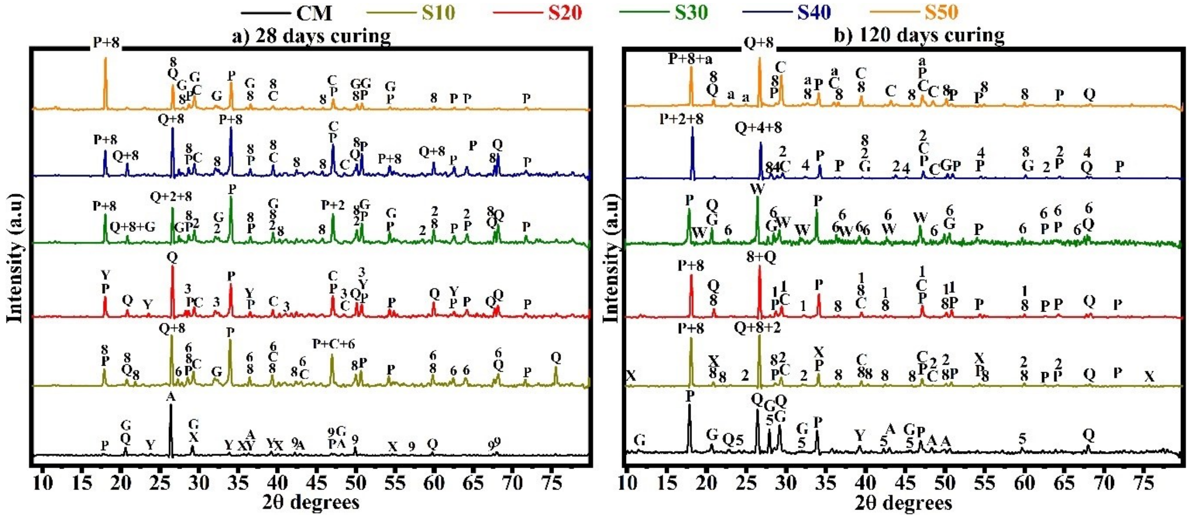

Fig. 10. XRD pattern of slag sand based cement mortar

Table 5. Details of the mineralogical compounds and their peak assignment

Compound	Peak assignment of bottom ash based mortar						Peak assignment of slag sand based mortar									
	28 days curing			120 days curing			28 days curing					120 days curing				
	CM	**B10**	**B20**	**CM**	**B10**	**B20**	**S10**	**S20**	**S30**	**S40**	**S50**	**S10**	**S20**	**S30**	**S40**	**S50**
Quartz (Silicon Oxide) (SiO_2)	Q	Q	Q	Q	Q	Q	Q	Q	Q	Q	Q	Q	Q	Q	Q	Q
Portlandite (Calcium Hydroxide) ($Ca(OH)_2$)	P	P	P	P		P	P	P	P	P	P	P	P	P	P	P
Rosenhahnite (Calcium Silicate Hydroxide) ($Ca_3(Si_3O_8(OH)_2)$)													1			
Hillebrandite (Calcium Silicate Hydroxide) ($Ca_2(SiO_3)(OH)_2)$									2			2			2	
Kamaishilite (Calcium Aluminium Silicate Hydroxide) ($Ca_2Al_2SiO_6(OH)_2$)			3					3								
Katoite, Silicatian, ($Ca_3Al_2(SiO)_4(OH)_8$) (Calcium Aluminium Silicate Hydroxide)															4	
Tobermorite (Calcium Silicate Hydroxide Hydrate) ($Ca_5(OH)_2Si_6O_{16}\cdot 4H_2O$)		T			T											
Calcium Silicate Hydroxide ($Ca_4Si_5O_{13.5}(OH)_2$)				5												
Xonotlite (Calcium Silicate Hydrate) ($Ca_6Si_6O_{17}(OH)_2$)	X											X				
Calcium Silicate Hydrate ($Ca_2SiO_4\cdot H_2O$)						6	6							6		
Chabazite (Calcium Aluminium Silicate Hydrate) ($Ca_2Al_4Si_8O_{24}\cdot 12H_2O$)		7			7											
Wairakite (Calcium Aluminium Silicate Hydrate) ($CaAl_2Si_4O_{12}\cdot 2H_2O$)					W									W		
Gismondine (Calcium Aluminum Silicate Hydrate) ($CaAl_2Si_2O_8.4H_2O$)			8			8	8		8	8	8	8	8		8	8
Calcium Aluminium Carbonate Silicate ($Ca_4Al_6Si_6O_{24}\cdot CO_3$)	9															
Calcite (Calcium Carbonate) ($CaCO_3$)			C			C	C	C		C	C	C	C		C	C
Aragonite (Calcium Carbonate) ($CaCO_3$)	A	A		A												
Dolomite ($CaMg(CO_3)_2$) (Calcium Magnesium Carbonate)					D											
Thaumasite ($CaSiO_3.CaCO_3.CaSO_4.15H2O$) Calcium Carbonate Silicate Sulfate Hydroxide Hydrate																a
Gypsum (Calcium Sulphate Hydrate) ($CaSO_4.2H_2O$)	G			G		G	G		G		G			G		
Yeelimite (Calcium Aluminium Oxide Sulphate) ($Ca_3Al_6O_{12}.CaSO_4$)	Y	Y	Y	Y	Y			Y								

3.4.2 Thermo gravimetric analysis (TGA)

The weight loss of the mortar samples with the increasing temperature was recorded through TGA and further TG/DTG curves were plotted. Fig. 11 a) and Fig. 11 b) presents the TG/DTG curves of 28 days and 120 days cured BA based mortar samples, respectively. Similarly, Fig. 11 c) and Fig. 11 d) shows the TG/DTG curves of 28 days and 120 days cured SS based mortar samples, respectively.

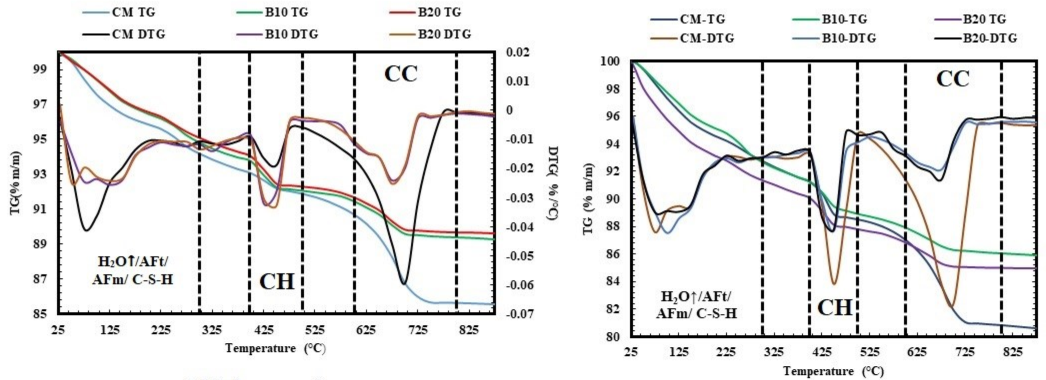

a) 28 days curing

b) 120 days curing

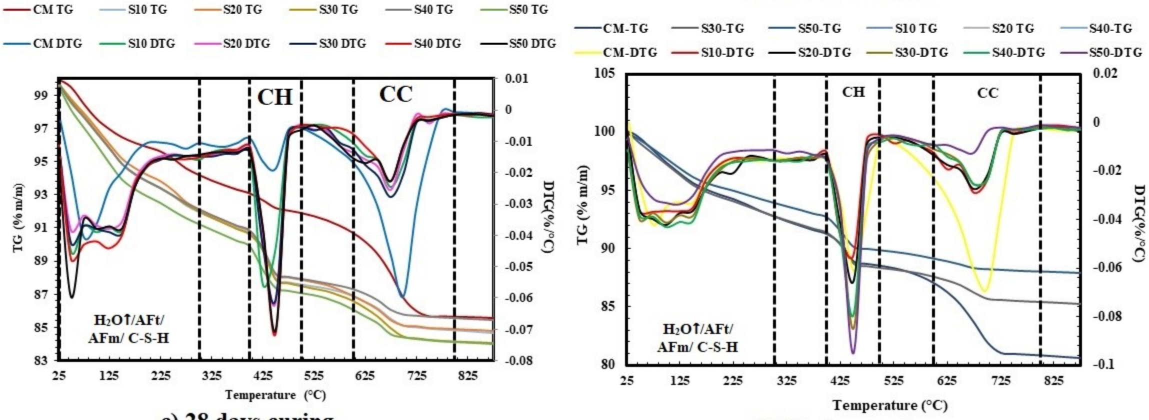

c) 28 days curing

d) 120 days curing

Fig. 11. TG and DTG curves of a) 28 days cured bottom ash based cement mortar, b) 120 days cured bottom ash based cement mortar, c) 28 days cured slag sand based cement mortar and d) 120 days cured slag sand based cement mortar

In the present study, the hydration products such as calcium hydroxide (CH), calcium carbonate (CC) and the water associated with other hydration products (WH) were quantified on the basis of their decomposition by weight loss at their specific temperature boundaries. The hydration products such as gypsum, ettringite, CSH, CASH, Friedel's salts, etc., were not calculated individually in this investigation due to overlapping temperature boundaries [32, 50, 51]. The measured values of CH, WH and CC are graphically presented in Fig. 12.

The quantified values of hydration products in the case of 28 days cured BA and SS based mortar samples exhibited an increasing CH content with the increasing percentage replacement of river sand by IBPs. This behavior confirmed the hindrance occurred to the hydration process caused by the excessive silica and alumina present in bottom ash. The additional calcium oxide obtained from the bottom ash particles and calcium rich slag sand particles causes an additional formation of portlandite, which is also responsible for the increasing trend of CH. On the other hand, the CH produced in control mortar (CM) readily takes part in hydration reaction and forms various other hydration products such as gypsum, ettringites and carbonates along with CSH. As a consequence, the quantified values of CH in CM recorded lowest at the curing age of 28 days.

It is also important to notice the variation of WH found to be in line with the consumption of CH. The control mortar showed the highest value of WH and BA based mortar samples recorded comparatively lesser WH due to the delayed hydration process. Whereas, the excessive calcium reserve in slag sand based mortars accelerates the hydration reactions to a greater extent which leads to the augmentation of WH with the increasing content of slag sand. This increment in the values of WH was observed till the optimum dosage of slag sand (S40) and is evident for the extensive formation of CSH/CASH gel which contributes to the performance enhancement of mortar.

The observed values of CC signify that the usage of IBPs (i.e., bottom ash and slag sand) drastically reduced the content of CC in the mortar which can be seen in Fig. 12. The preferential formation of gypsum and ettringite in the control mortar can also be observed through an intensive endothermic peak existing in DTG curve within 150°C. Whereas, the IBPs based mortar showed relatively broader endothermic peaks which signifies the development of additional CSH and CASH with a limited amount of gypsum and ettringite.

By investigating the TGA results of 120 days cured mortars, the formation of CH was found to be continuing with the curing age. Whereas a higher consumption of CH for the primary and secondary hydration reactions was found in IBPs based mortars, owing to the formation of supplementary CSH/CASH gels. This development can also be noticed through the increased value of WH along with broadened endothermic peaks observed in the temperature range of 110 °C-300 °C. Similar to 28 days results, the formation of WH at 120 days curing was found to be slightly higher for optimized IBPs based mortar (i.e., B10 and S40) which is due to the optimized content of IBPs favorable for undergoing reactions efficiently. In addition to these, the quantified values of CC in 120 days cured IBPs based mortar samples were also found to be significantly lower than the control mortar.

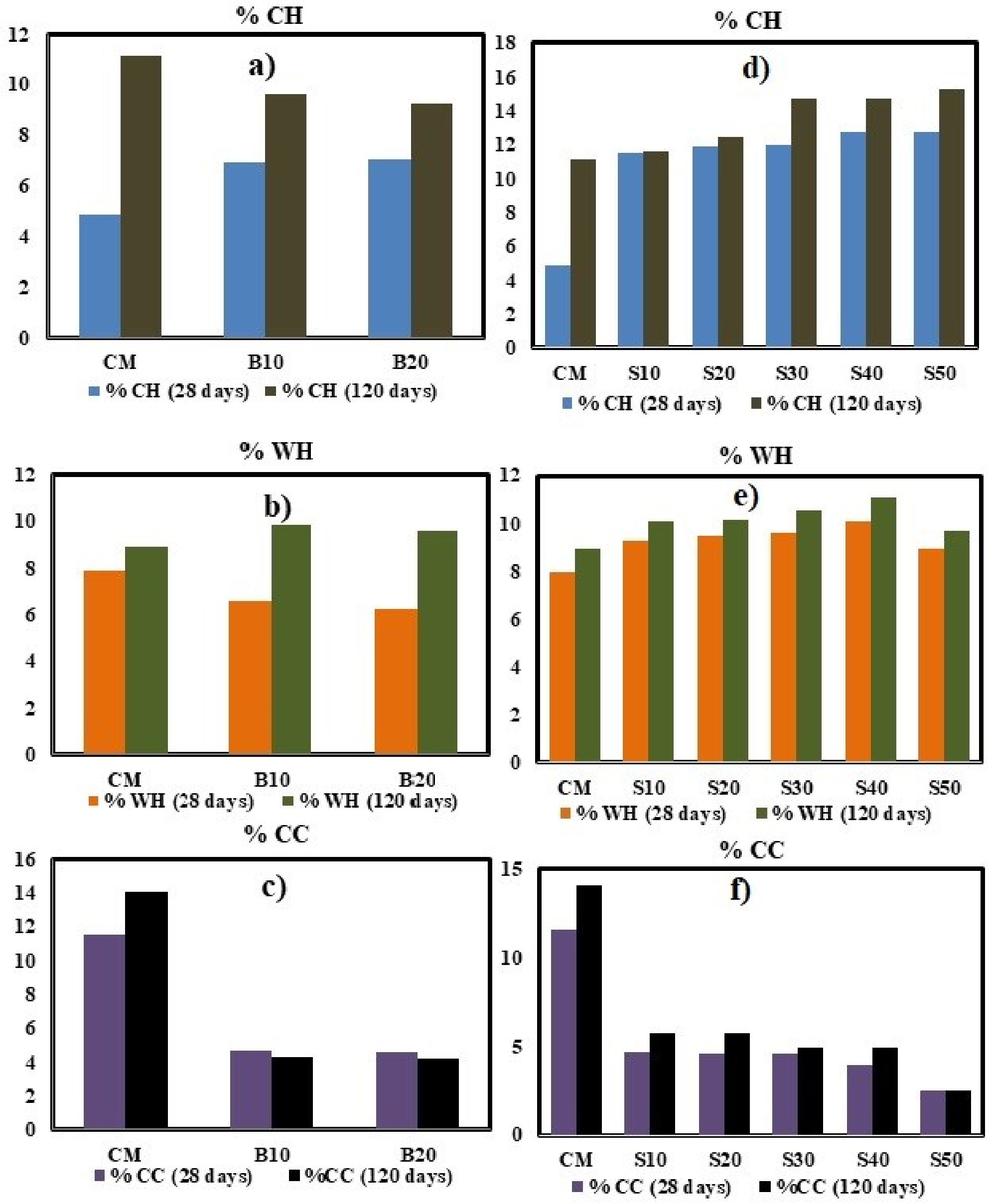

Fig. 12. Phase compounds formed in bottom ash based mortar [(a) CH; (b) WH; c) CC] and slag sand based mortar [(d) CH; (e) WH; (f) CC] after 28 days and 120 days of curing

3.4.3 Fourier transform infrared spectroscopy (FT-IR)

Fig. 13 a) and Fig. 13 b) presents the FTIR spectra of BA based cement mortar after 28 days and 120 days of curing, respectively. Further, Fig. 14 a) and Fig. 14 b) presents the FTIR spectra of SS based cement mortar at a curing age of 28 days and 120 days, respectively. The details regarding the functional group assignment associated to different wavenumbers are tabulated in Table 6.

The major functional groups visible in all types of mortars were found to be similar in the obtained FTIR spectra. The vibration band associated to Si-O-Si asymmetric stretching visible in the wavenumber range of 900-1000 cm^{-1} is more prominent and consistent in all types of mortars produced. This Si-O-Si asymmetric stretching band showed a significant shift towards a lower wavenumber by the usage of IBPs such as bottom ash and slag sand in cement mortar. The BA based mortar showed a shift from 1001.69 cm^{-1} to 954.48 cm^{-1} and from 993.48 cm^{-1} to 960.63 cm^{-1} by the end of 28 days and 120 days of curing, respectively. Similarly, the SS based mortar records a shift from 1001.69 cm^{-1} to 956.63 cm^{-1} and from 993.48 cm^{-1} to 942.16 cm^{-1} by the end of 28 days and 120 days of curing, respectively. This reduction in the wavenumber associated to Si-O-Si asymmetric stretching band signifies the formation of stronger bonds which is attributed to the synergetic effect of improved particle packing and secondary hydration reactions imparted by the usage of IBPs. The enhanced degree of particle packing eases the reactivity of minerals, leading to the formation of additional hydration products. The pozzolanic reactivity offered by the particles of IBPs enables secondary hydration reactions which produce additional C-S-H and C-A-S-H phases.

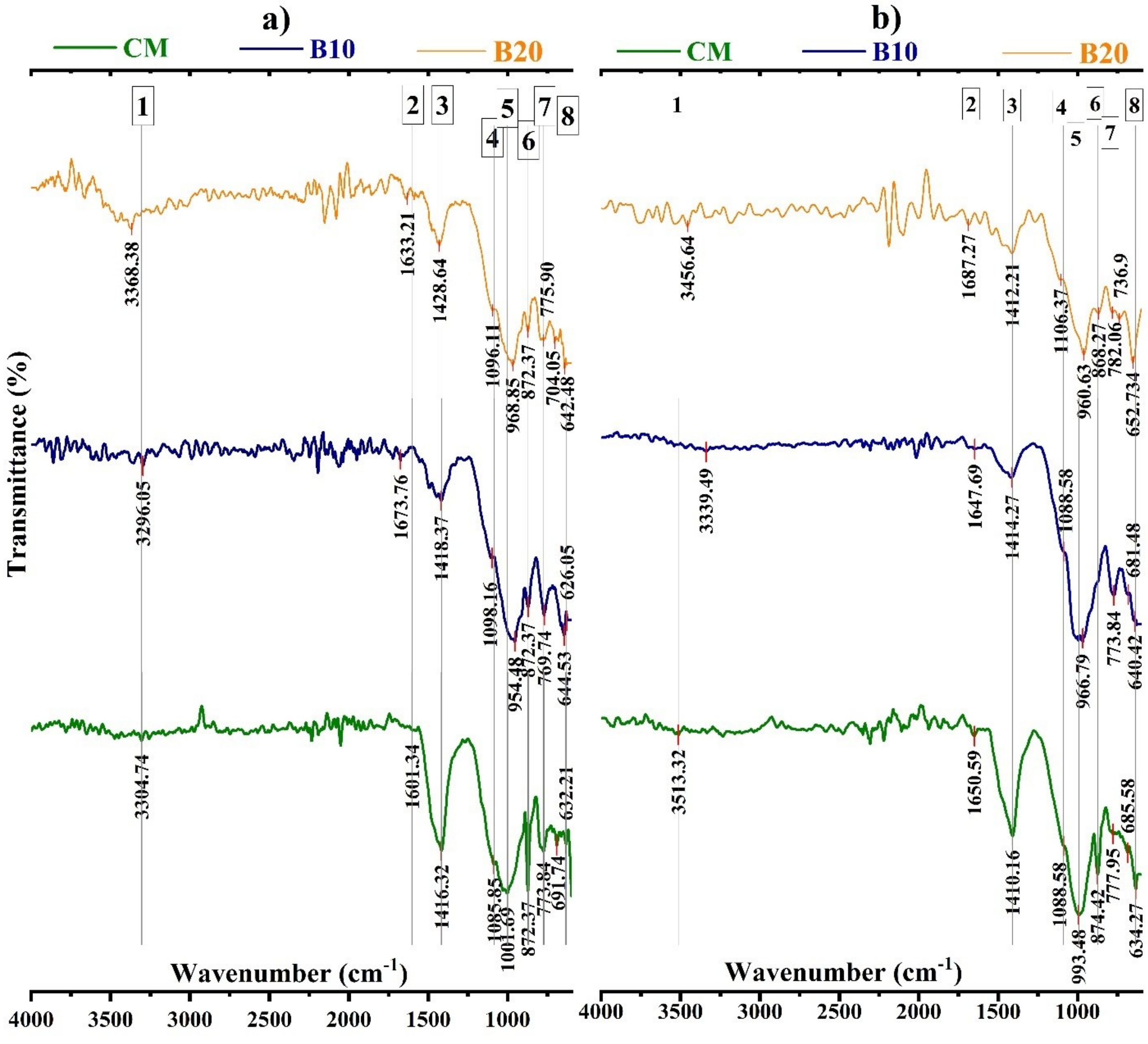

Fig. 13. FTIR spectra of control and BA based mortars at a curing age of a) 28 days and b) 120 days

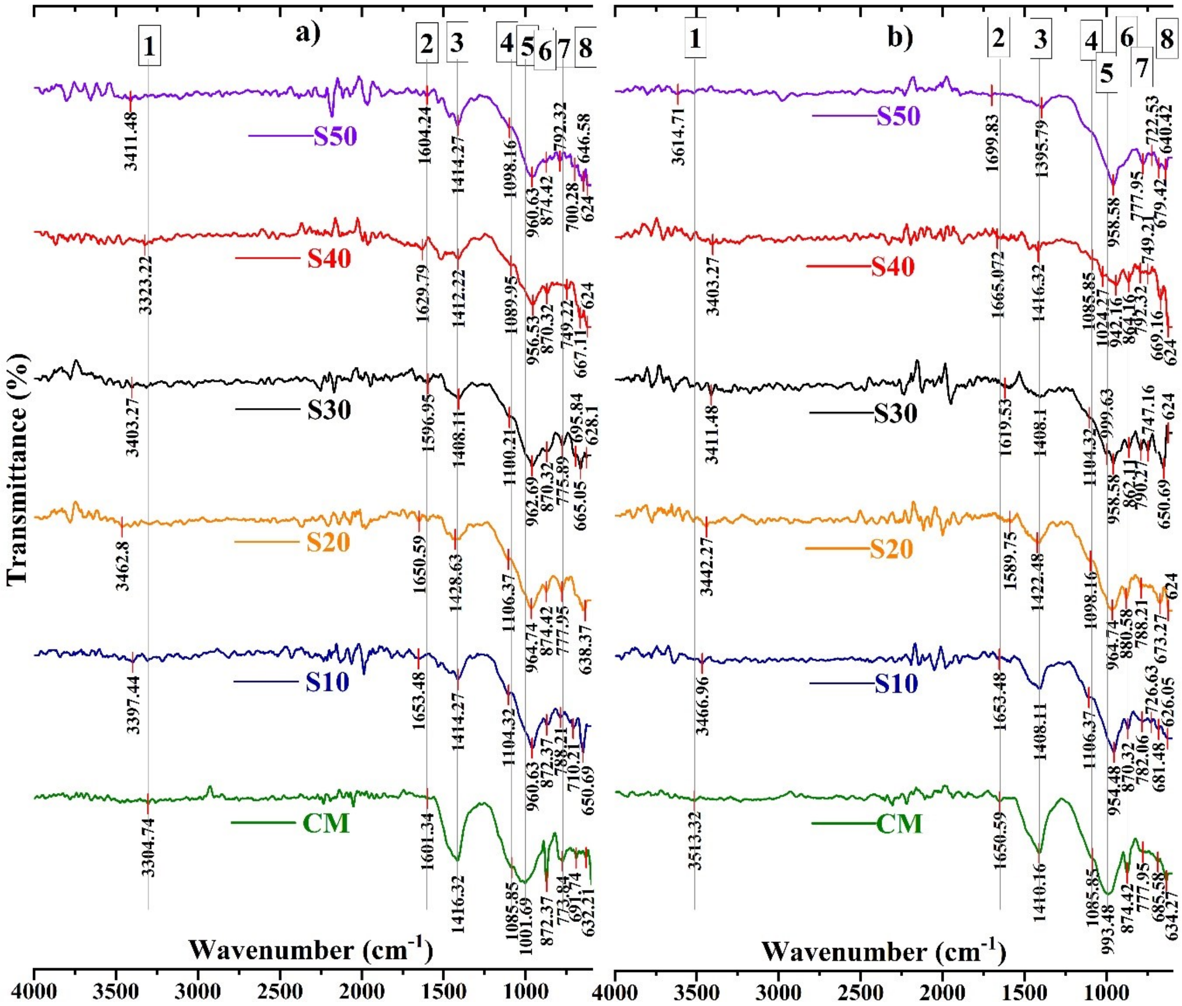

Fig. 14. FTIR spectra of control and SS based mortars at a curing age of a) 28 days and b) 120 days

The vibration band corresponding to Si-O-Si/Al symmetric stretching was also prominently observed in the produced mortars at a wavenumber range of 675-800 cm^{-1}. These vibration bands are found slightly broad and intense in the case of IBPs based mortars both at 28 days and 120 days of curing. This development is due to the extensive formation of CSH and CASH phases by the action of secondary hydration reactions facilitated by IBPs particles which create stronger bonds and hence better microstructure. However, there is no considerable shift observed in the vibration bands associated to Si-O-Si/Al symmetric stretching by the implementation of IBPs. All these findings are found in line with the XRD analysis data.

It is also important to notice the significant reduction in the intensities of vibration bands related to O-C-O asymmetric stretching and O-C-O bending with the usage of IBPs in both 28 and 120 days cured mortars. This feature assisted the IBPs based mortars to have a quality microstructure irrespective of delayed hydration lag in the early stages of curing. These findings are in good alignment with the TGA and SEM results presented.

Table 6: Particulars of the functional group assignment at different wavenumbers

Notation No	Age of curing	Wavenumber (cm^{-1}) corresponding to different peaks								Functional group assignment
		CM	B10	B20	S10	S20	S30	S40	S50	
1	28	3304.94	3296.05	3368.38	3397.44	3462.80	3403.27	3323.22	3411.48	O-H asymmetric stretching
	120	3513.32	3339.49	3456.64	3466.96	3442.27	3411.48	3403.27	3614.71	
2	28	1601.34	1673.76	1633.21	1653.48	1650.59	1596.95	1629.79	1604.24	O-H asymmetric bending
	120	1650.59	1647.69	1687.27	1653.48	1589.75	1619.53	1665.07	1699.83	
3	28	1416.32	1418.37	1428.64	1414.27	1428.63	1408.11	1412.22	1414.27	O-C-O asymmetric stretching
	120	1410.16	1414.27	1412.21	1408.11	1422.48	1408.10	1416.32	1395.79	
4	28	1085.85	1098.16	1096.11	1104.32	1106.37	1100.21	1089.95	1098.16	S-O stretching
	120	1088.58	1088.58	1106.37	1106.37	1098.16	1104.32	1085.85	-	
5	28	1001.69	954.48	968.85	960.63	964.74	962.69	956.53	960.63	Si-O-Si asymmetric stretching
	120	-	-	-	-	-	999.63	1024.27	-	
		993.48	966.79	960.63	954.48	964.74	958.58	942.16	958.58	
6	28	872.37	872.37	872.37	872.37	874.42	870.32	870.32	874.42	O-C-O bending
	120	874.42	-	868.27	870.32	880.58	862.11	864.16	-	
7	28	773.84	769.74	775.90	788.21	777.95	775.89	749.22	792.32	Si-O-Si/Al symmetric stretch
		691.74	-	704.05	710.21	-	695.84	-	700.28	
	120	777.95	773.84	782.06	782.06	788.21	790.27	792.32	777.95	
		-	-	736.90	726.63	-	747.16	749.21	722.53	
		685.58	681.48	-	681.48	-	-	-	679.42	
8	28	632.21	644.53	642.48	650.69	638.37	665.05	667.11	646.58	S-O bending
		-	626.05	-	-	-	628.1	624	624	
	120	634.27	640.42	652.73	626.05	624	624	624	640.42	
		-	-	-	-	673.27	650.69	669.16	-	

3.4.4 Scanning electron microscopy (SEM) and energy dispersive x-ray spectroscopy (EDS)

The microstructural development and the morphology of hydrated control and optimized IBPs mortars (i.e., CM, B10 and S40) were examined through SEM. The scanning electron micrographs of 28 days and 120 days cured mortar samples are presented in Fig. 15 and Fig. 16, respectively. The compounds in the micrographs were visually identified based on their structure, shape, color and texture [52]. Further, the EDS analysis results highlighting the elemental composition of these mortar samples are tabulated in Table 7. Fig. 17 shows a typical image on which EDS analysis was conducted.

The Ca/Si atomic ratio was extracted from the obtained EDS results and used to study the extent of hydration products formation such as calcium hydroxide (CH) and CSH. Since the development of CSH phases highly relies on calcium (Ca) and silicate (Si) ions present in pore solution, the Ca/Si atomic ratio signifies the extent of calcium hydroxide (CH) and CSH formation[53]. The cement matrix with lesser Ca/Si atomic ratio indicates a dense microstructure, owing to the formation of greater and stronger CSH network [54].

The SEM micrographs of 28 days cured IBPs based mortar samples appear to have a dense microstructure with reduced number of voids in comparison with the control mortar. This could be due to the improved particle packing achieved with the usage of IBPs, which contributes to the effective hydration reactions which eases the process of pore refinement. The occurrence of CSH gels in substantial amounts with lesser Ca/Si atomic ratio confirms this development. However there also observed a significant amount of unutilized CH in IBPs based mortars which is possibly due to decelerated hydration reaction caused by the excessive silica and alumina content in BA based mortars. In contrast, the presence of excessive CH in SS based mortars is attributed to the additional calcium oxide particles added from the slag sand particles. It is also important to observe that the SEM micrographs of control mortar shows higher formation of CC and ettringites in comparison to that of IBPs based mortars.

Similar kind of advancements were observed in the microstructure of 120 days cured mortar samples. However, the microstructure of mortars appeared denser than 28 days cured ones due to the continuation of hydration process with the curing age. In addition to these, IBPs based mortars showed a much denser microstructure with well-developed CSH/CASH network and minimal amount of ettringites and CC. The reduction in Ca/Si atomic ratio of IBPs based mortars from 28 days to 120 days also confirms the effective conversion of CH into CSH/CASH phases. The additional formation of CSH and CASH phases in IBPs based mortars observed in the SEM micrographs helped in improving the microstructure. The bottom ash based mortar showed an extensive formation of CSH and CASH phases in the form of globular, spongy, fibrous and amorphous network. Similarly, fibrous and amorphous structured CSH and CASH phases were predominantly formed in slag sand based mortars. These distinctly formed CSH and CASH phases beyond 28 days of curing in IBPs based mortars are evident for the formation of additional hydration products through secondary hydration reactions, facilitated by the reactive finer fractions present in IBPs. This constructive development densified the IBPs mortar microstructure and helped to perform superior than conventional mortar.

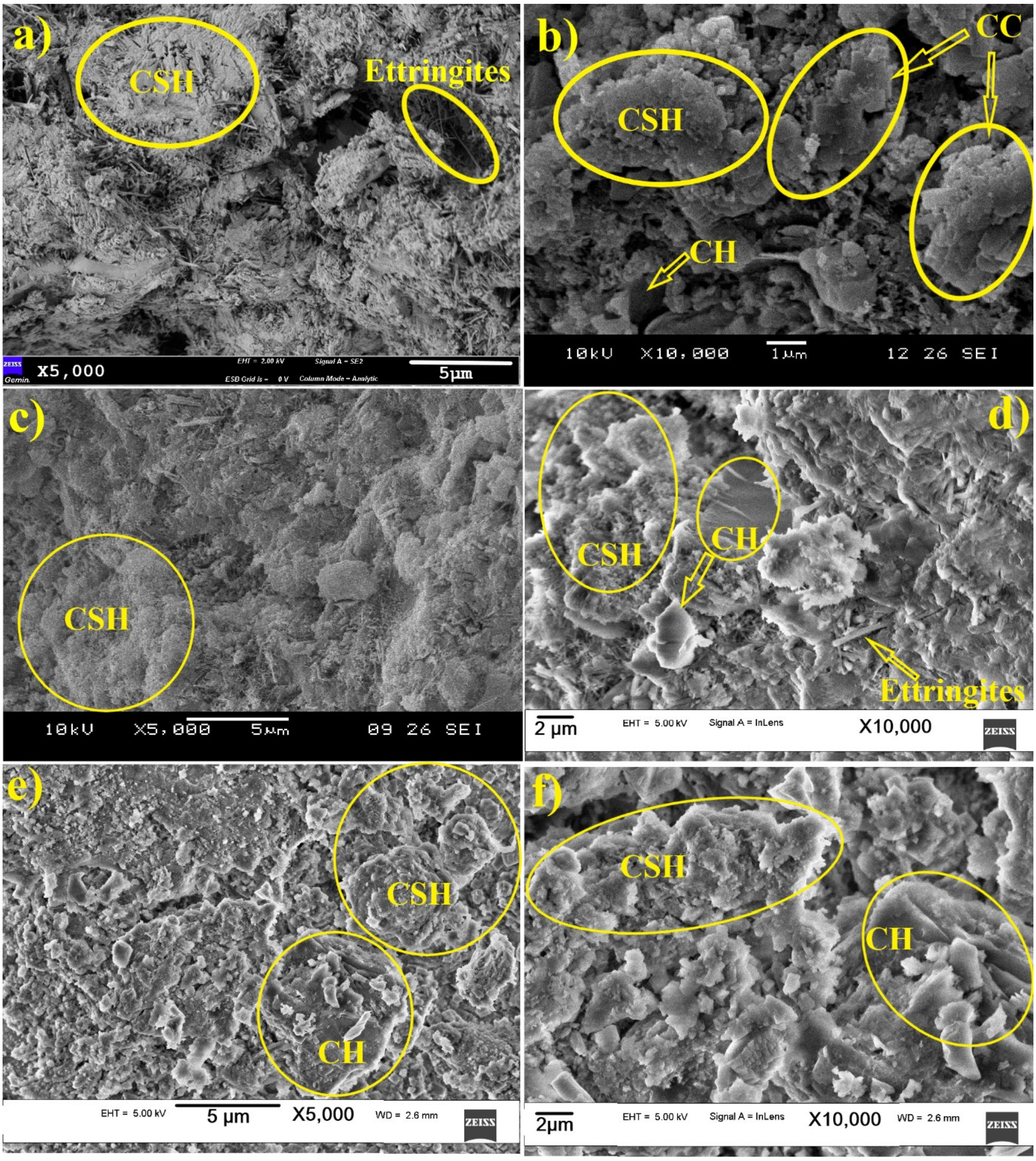

Fig. 15. Scanning electron micrograph of control (CM) [a), b)], B10 [c), d)] and S40 [e), f)] mortar at 28 days of curing

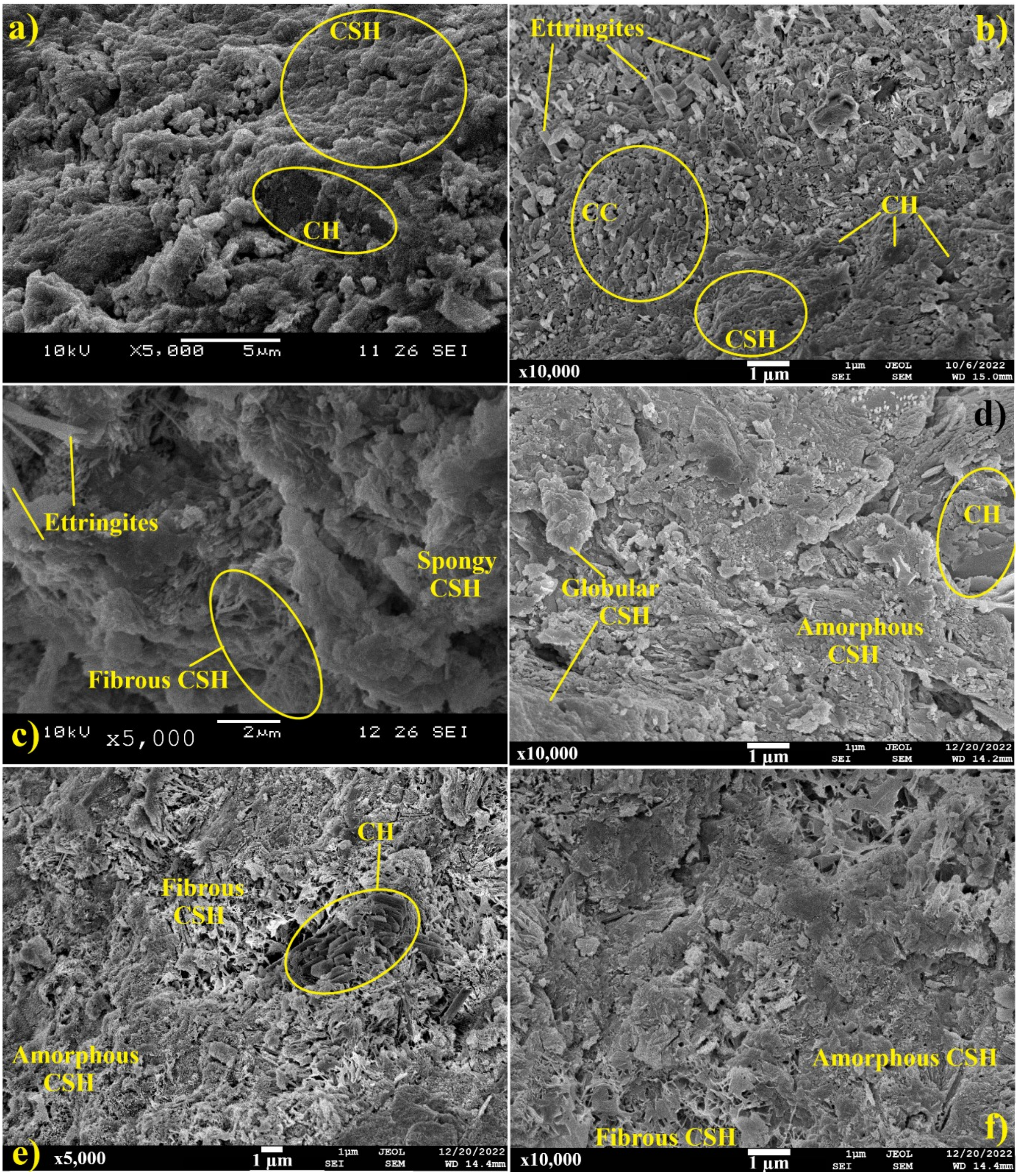

Fig. 16. Scanning electron micrograph of control (CM) [a), b)], B10 [c), d)] and S40 [e), f)] mortar at 120 days of curing

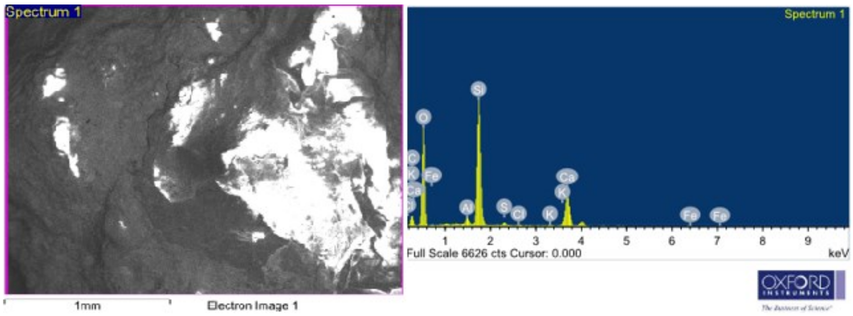

Fig. 17. Typical image showing the EDS analysis of mortar sample

Table 7: EDS elemental analysis of produced mortars at 28 days and 120 days of curing

Element	Atomic weight (%) of 28 days cured mortar			Atomic weight (%) of 120 days cured mortar		
	CM	**B10**	**S40**	**CM**	**B10**	**S40**
C	15.43	22.84	18.32	16.00	19.10	19.10
Ca	14.99	14.49	17.98	9.85	12.975	16.175
O	58.2	55.37	56.58	54.60	55.55	54.11
Al	5.22	0.5	0.74	2.55	1.40	1.05
Si	5.29	6.03	5.43	4.05	5.75	5.10
Mg	0.16	-	0.38	-	0.10	0.167
S	0.28	0.28	0.23	10.65	0.80	0.90
Cl	0.03	0.11	-	-	-	-
K	0.11	0.1	0.03	0.3	0.10	0.05
Fe	0.3	0.28	0.22	1.75	0.30	0.10
Na	-	-	0.09	0.25	0.05	-
Ti	-	-	-	-	0.45	0.35
Mn	-	-	-	-	2.20	1.60
Zr	-	-	-	-	1.25	1.30
Ca/Si	**2.836**	**2.402**	**3.311**	**2.432**	**2.256**	**3.171**

4. Conclusions

The conclusions drawn from the present investigation are presented as follows,

- The primary investigations on the bottom ash and slag sand showed comparable properties with river sand and hence could be utilized as a partial substitute to river sand in developing cementitious composites.
- The mortar produced with IBPs presented lower workability characteristics and the study confirms the flowability of about 15 cm can be easily achieved with the aid of superplasticizers.
- The usage of IBPs as fine aggregate found influencing the setting of mortars. The experiments revealed that the inclusion of BA retards the setting process by around 2 hours at their optimum level usage. Whereas, the inclusion of SS accelerated the setting process by an hour approximately at optimum level usage. Thus, the usage of these mortars can be made as per the required application suitably or a compatible retarder/ accelerator can be equipped to regulate the setting time.
- The inclusion of IBPs as fine aggregates in mortar enhanced the degree of particle packing and secondary hydration activity. This further assists in enhancing the performance, observed in terms of compressive strength, water absorption and permeable porosity. The performance increment of slag sand based mortar is quite significant when compared with the bottom ash based mortars. Hence, these IBPs improve the service life of structure by encasing the load bearing structure effectively from surrounding exposures that affect the durability of structure.
- The experimental findings confirm that, in conjunction with the degree of particle packing and the hydration mechanism, the dry density of produced mortars greatly relies on the specific gravity of ingredients and the UPV highly depends on the extent of homogeneity in the mix. The reduced dry density and improved UPV at optimised proportion of IBPs confirms the reduction in density is due to lower specific gravity associated with the alternative used for river sand. Further, the reduced dry density contributes in reducing the dead load of the structure.
- The advanced characterization studies such as SEM-EDS, XRD, TGA and FTIR analysis confirms the performance enhancement seen in IBPs based mortars. The lowering Ca/Si ratio through EDS, formation of additional CSH and CASH phases through XRD, increased consumption of CH along with augmented values of WH through TGA and occurrence of additional Si-O-Si/Al stretching bands with considerable shifts towards the lower wavenumber through FTIR confirms the occurrence of secondary hydration reactions by the IBPs particles that helped in improving the microstructure (observed through SEM) and overall performance of engineered cement mortar further.

The conclusions drawn from the experimental findings recommend the usage of bottom ash up to 10% and slag sand up to 40% as a feasible alternative to river sand without compromising the performance of cement mortar.

Declaration of Competing Interest

The authors declare that they have no conflict of interest, financial interests or personal relationships that could have appeared to influence the research work reported in this article.

Acknowledgements

The authors acknowledge the experimental facility provided by Department of Civil Engineering, Department of Metallurgical and Materials Engineering and Central Research Facility (CRF) at National Institute of Technology Karnataka, Surathkal, India. The authors also extend their acknowledgements to PURSE research centre at Mangalore University, Karnataka, India.

References

[1] Hussin JM, Rahman IA, Memon AH (2013) The way forward in sustainable construction: issues and challenges. International Journal of Advances in Applied Sciences 2:15–24

[2] Oktay H, Yumrutas R, Akpolat A (2015) Mechanical and thermophysical properties of lightweight aggregate concretes. Construction and Building Materials 96:217–225

[3] Dhir RK, de Brito J, Silva R V., Lye CQ (2019) Processing of Recycled Aggregates. Sustainable Construction Materials: 57–88. https://doi.org/10.1016/b978-0-08-100985-7.00004-2

[4] Drew LJ, Langer WH, Sachs JS (2002) Environmentalism and natural aggregate mining. Natural Resources Research 11:19–28. https://doi.org/10.1023/A:1014283519471

[5] Dan Gavriletea M (2017) Environmental impacts of sand exploitation. Analysis of sand market. Sustainability (Switzerland) 9:. https://doi.org/10.3390/su9071118

[6] Suresh S, Revathi J (2016) Effect of M-Sand on Setting Time of High Performance Concrete. Asian Journal of Research in Social Sciences and Humanities 6:1648. https://doi.org/10.5958/2249-7315.2016.01118.7

[7] Jayswal S, Mungule M (2018) Assessment of M-Sand As Potential Substitute for Natural Sand in Concrete. In: International Conference on 2019, pp 7-8.

[8] Sudha C, Kottuppillil AK, Ravichandran PT, Divya Krishnan K (2016) Study on Mechanical Properties of Concrete with Manufactured Sand and Bagasse Ash. Indian Journal of Science and Technology 9: 1-6. https://doi.org/10.17485/ijst/2016/v9i34/95867

[9] Pilegis M, Gardner D, Lark R (2016) An investigation into the use of manufactured sand as a 100% replacement for fine aggregate in concrete. Materials 9:440. https://doi.org/10.3390/ma9060440

[10] Li B, Ke G, Zhou M (2011) Influence of manufactured sand characteristics on strength and abrasion resistance of pavement cement concrete. Construction and Building Materials 25:3849–3853. https://doi.org/10.1016/j.conbuildmat.2011.04.004

[11] Elavenil S, Engg C (2013) Manufactured Sand, A Solution And An Alternative To River Sand And In Concrete Manufacturing. 2:20–24

[12] Alyami M, Hakeem IY, Amin M, Zeyad AM, Tayeh BA, Agwa IS (2023) Effect of agricultural olive, rice husk and sugarcane leaf waste ashes on sustainable ultra-high-performance concrete. Journal of Building Engineering 72:106689

[13] Alyami M, Mydin MAO, Zeyad AM, Majeed SS, Tayeh BA (2023) Influence of wastepaper sludge ash as partial cement replacement on the properties of lightweight foamed concrete. Journal of Building Engineering 79:107893

[14] Golewski GL (2023) Mechanical properties and brittleness of concrete made by combined fly ash, silica fume and nanosilica with ordinary Portland cement. AIMS Mater Sci 10:390–404

[15] Zeyad AM, Shubaili M, Abutaleb A (2023) Using volcanic pumice dust to produce high-strength self-curing concrete in hot weather regions. Case Studies in Construction Materials 18:e01927

[16] Zeyad AM (2023) Sustainable Concrete Production: Incorporating recycled wastewater as a green building material. Construction and Building Materials 407:133522

[17] Golewski GL (2023) Assessing of water absorption on concrete composites containing fly ash up to 30% in regards to structures completely immersed in water. Case Studies in Construction Materials 19:e02337

[18] Wang L, Zhang P, Golewski G, Guan J (2023) Fabrication and properties of concrete containing industrial waste. Frontiers in Materials 10:1169715

[19] Elbasri OMM, Nser S, Shubaili M, Abdullah GMS, Zeyad AM (2022) Performance of self-compacting concrete incorporating wastepaper sludge ash and pulverized fuel ash as partial substitutes. Case Studies in Construction Materials 17:e01459

[20] Golewski GL (2023) Concrete Composites Based on Quaternary Blended Cements with a Reduced Width of Initial Microcracks. Applied Sciences 13:7338

[21] Golewski GL (2023) The effect of the addition of coal fly ash (CFA) on the control of water movement within the structure of the concrete. Materials 16:5218

[22] Juric B, Hanzic L, Ilic R, Samec N (2006) Utilization of municipal solid waste bottom ash and recycled aggregate in concrete. Waste Management 26:1436–1442

[23] Patil AR, Sathe SB (2021) Feasibility of sustainable construction materials for concrete paving blocks: A review on waste foundry sand and other materials. Materials Today: Proceedings 43:1552–1561

[24] Yoshizawa S, Tanaka M, Shekdar AV (2004) Global Trends in Waste Generation. In: Recycling, Waste Treatment and Clean Technology, TMS Mineral, Metals and Materials Publishers:1541-1552.

[25] Yin K, Ahamed A, Lisak G (2018) Environmental perspectives of recycling various combustion ashes in cement production–A review. Waste Management 78:401–416

[26] Rashad AM (2018) An overview on rheology, mechanical properties and durability of high-volume slag used as a cement replacement in paste, mortar and concrete. Construction and Building Materials 187:89–117

[27] ASTM C150/C150M-22 (2022) Standard specification for portland cement. West Conshohocken, PA: ASTM International, approved July 1, 2022, Published July 2022, https://doi.org/10.1520/C0150_C0150M-22.

[28] BIS (2012) Indian Standard Drinking Water Specification (Second Revision). Bureau of Indian Standards IS 10500:1–11

[29] Bureau of Indian Standards (2003) IS 2645: 2003 Integral Waterproofing Compounds for Cement Mortar and Concrete -Specification. 16

[30] Bureau of Indian Standards (1993) IS 9103: 1999 Indian standard concrete admixtures-specifications

[31] EN BS (2005) 1052-3. BS EN 196-1: Methods of testing cement. Determination of strength. https://doi.org/10.3403/30291447U

[32] Snehal K, Das BB, Akanksha M (2020) Early age, hydration, mechanical and microstructure properties of nano-silica blended cementitious composites. Construction and Building Materials 233:117212

[33] Zhang J, Scherer GW (2011) Comparison of methods for arresting hydration of cement. Cement and Concrete Research 41:1024–1036

[34] EN BS (1999) 1015-3. Methods of Test for Mortar for Masonry—Part 3: Determination of Consistence of Fresh Mortar (by Flow Table). NBN, Bureau for Standardisation: Brussels, Belgium

[35] ASTM C403 (2005) ASTM C 403, "Standard Test Method for Time of Setting of Concrete Mixtures by Penetration Resistance," ASTM C 403-95, Annual Book of ASTM Standards, American Society for Testing and Materials, Pennsylvania, 1998. ASTM. 1–7. https://doi.org/10.1520/C0403

[36] BIS (2005) Indian Standard IS: 4031 (Part 6)-1988 (Reaffirmed 2005). Methods Of Physical Tests For Hydraulic Cement-Part 6: Determination of compressive strength of hydraulic cement other than masonry cement (First Revision).

[37] EN BS (1999) 1015-10, 1999. Methods of test for mortar for masonry—Part 10: Determination of dry bulk density of hardened mortar. Br Stand[29] BS EN 1011–1015

[38] Safiuddin M, Hearn N (2005) Comparison of ASTM saturation techniques for measuring the permeable porosity of concrete. Cement and Concrete Research 35:1008–1013

[39] Das BB, Singh DN, Pandey SP (2010) A comparative study for determining pore volume of concrete. Indian Concrete Journal 84:7

[40] Bureau of Indian Standards (2018) IS 516: Part 5/Sec 1-2018 Hardened Concrete — Methods of Test, Non-destructive Testing of Concrete, Section 1, Ultrasonic Pulse Velocity Testing, First Revision.

[41] BS 1881-122 BS (2011) Testing concrete-Method for determination of water absorption.

[42] Singh LP, Goel A, Bhattacharyya SK, Sharma U, Mishra G (2015) Hydration studies of cementitious material using silica nanoparticles. Journal of Advanced Concrete Technology 13:345–354

[43] Jain J, Neithalath N (2009) Analysis of calcium leaching behavior of plain and modified cement pastes in pure water. Cement and Concrete Composites 31:176–185

[44] Singh LP, Bhattacharyya SK, Mishra G, Ahalawat S (2012) Reduction of calcium leaching in cement hydration process using nanomaterials. Materials Technology 27:233–238

[45] Singh LP, Bhattacharyya SK, Ahalawat S (2012) Preparation of size controlled silica nano particles and its functional role in cementitious system. Journal of Advanced Concrete Technology 10:345–352

[46] Jayalath A, San Nicolas R, Sofi M, Shanks R, Ngo T, Aye L, Mendis P (2016) Properties of cementitious mortar and concrete containing micro-encapsulated phase change materials. Construction and Building Materials 120:408–417

[47] Dinger DR, Funk JE (1997) Particle-packing phenomena and their application in materials processing. Mrs Bulletin 22:19–23

[48] User Guide Elkem Materials Mixture Analyser-EMMA, Version-1.

[49] IS 13311: Part 1-1992 Method of Non-destructive testing of concrete, Part-1: Ultrasonic pulse velocity. Bureau of Indian Standards: 1–7

[50] Snehal K, Das BB (2022) Pozzolanic reactivity and drying shrinkage characteristics of optimized blended cementitious composites comprising of Nano-Silica particles. Construction and Building Materials 316:125796

[51] Snehal K, Das BB (2021) Acid, alkali and chloride resistance of binary, ternary and quaternary blended cementitious mortar integrated with nano-silica particles. Cement and Concrete Composites 123:104214

[52] Patil AY, Banapurmath NR, EP S, Chitawadagi M V, Khan TMY, Badruddin IA, Kamangar S (2020) Multi-scale study on mechanical property and strength of new green sand (Poly Lactic Acid) as replacement of fine aggregate in concrete mix. Symmetry 12:1823

[53] Hu Q, Aboustait M, Kim T, Ley MT, Hanan JC, Bullard J, Winarski R, Rose V (2016) Direct three-dimensional observation of the microstructure and chemistry of C3S hydration. Cement and concrete research 88:157–169

[54] Goudar SK, Sumukh EP, Das BB (2023) Implication of high-volume mineral admixture on mechanical properties and microstructure at steel-concrete interface. The Indian Concrete Journal 97:17-27.